Numerical Simulation of a Downburst-Producing Intense Convective Storm : Some Preliminary Results (Mathematical Aspects of Thermal Convection Dynamics : Structure of Flow Fields)

AUTHOR(S):

Guo, Xueliang; Niino, Hiroshi; Kimura, Ryuji

数理解析研究所講究録
1115巻 1999年 165-180

Numerical Simulation of a Downburst-Producing Intense Convective Storm: Some Preliminary Results

Xueliang Guo, Hiroshi Niino and Ryuji Kimura
Ocean Research Institute, University of Tokyo, Minamidai,Nakano-ku, Tokyo 164-8639,Japan

Abstract

A downburst-producing convective storm on 8 September 1994 in Saitama Prefecture in Japan was reproduced by a three-dimensional cloud model. The simulated results such as descending precipitation cores, decreasing of temperature at the surface, intensity of the divergent wind speed near surface and the development of multiple downbursts were well consistent with that observed. The mechanism of development of the downburst was investigated based on the numerical simulation and found that the formation of hail/graupel played a vital important role in developing the wet microburst. The effects of adiabatic warming of descending motion, diabatic cooling due to melting and evaporation and environmental condition on the formation of downdraft were also discussed in this study.

1. Introduction

Thermal convection is one of the very important atmospheric vertical currents induced by extreme surface heating. Depending on humidity condition, thermal convection in atmosphere can be subdivided into two basic categories: dry and wet thermal convection. Convective thunderstorms are a kinds of wet convections and often contain intense small-scale downdrafts,termed "downburst", that are a significant hazard to aviation (Fujita and Caracena 1977).

According to previous observational study conducted by Byers and Braham (1949) during the Thunderstorm Project, the key to the development of downdraft is entrainment within the updraft and precipitation loading, and updraft overshooting and its subsequent descent is another possible cause of downdraft development. The downdraft was observed to continue below the cloud base, reaching close to the surface of the earth, where it spread out as a layer of cold air. The maximum strength of downdraft was observed to occur near the middle levels of cloud and the downdraft width was frequently about 1.2 km.

Downdraft strengths were also found to have little or no variation with height, except, of course, in its approach to zero near the surface of the earth in the GATE and hurricanes data (Zipser and Lemone,1980).

Fujita and Wakimoto (1983) defined the downbursts as " a strong downdraft which induces an outburst of damaging winds near the ground ". Based on their space and time scales, the downburst was subdivided into macro- and micro-bursts. The macroburst was defined to having an outflow size greater than 4 km and life time of 5-20 minutes, while the microburst was defined as having an outflow size less than 4 km and a life time of 2-5 minutes. Further, " dry microburst" was termed if the surface precipitation is less than 0.01 inches; otherwise it was termed " wet microburst".

A distinguishing characteristic of downburst is its continued intensification as it descends below the melting level or cloud base and the occurrence of its peak magnitude close to the earth's surface. But only under certain conditions, the downdraft intensifies as it descends. In a one-dimensional model, it is found that a strong downdraft may develop if

the lapse rate of temperature is close to the dry adiabatic (Harris, 1977; Srivastawa,1985). With such a lapse rate, an intense downdraft can occur with a very low rainfall rate or precipitation content. These kinds of intense downdrafts can be called "dry downburst". In a more stable condition of thermal stratification, higher rainfall rates or precipitation contents are required to drive intense downdraft, that is, these intense downdrafts are "wet downburst".

Observations also show that wet and dry downburst occurred in some different conditions: 83% of the microbursts observed during JAWS (Joint Airport Weather Study), conducted in the Denver area during the summer months of 1982, were dry, while 64% of the microbursts identified during NIMROD (Northern Illinois Meteorological Research on Downburst), conducted in the Chicago area during May and June of 1978, were wet (Fujita,1985). In the summer, the Denver area often has high cloud bases and deep near dry-adiabatic sub-cloud layer. At least two wet microbursts were also found to occur in JAWS in rather stable stratification, with the lapse rate of temperature somewhat less than 6 K km^{-1} and were accompanied with heavy precipitation.

Evaporative cooling of precipitation is thought as being the primary driving mechanism for most dry microbursts. There is no general agreement on the physical mechanism responsible for wet downburts. The difficulty in explaining them is due to their occurrence in relatively stable lapse rates, sometime approaching the wet adiabatic. The possible physical mechanisms for the wet downburst may involve dynamical or additional microphysical effects besides the evaporation of raindrops considered in dry downburst.

Multi-dimensional numerical models can aid us to understand the mechanism of downburst phenomena. The models used to study microbursts can be generally categorized into two types: subcloud models,in which some sort of forcing is imposed in an elevated region of the domain (e.g., Teske and Lewellen 1977; Srivastava 1985; Proctor 1988,1989; Anderson et al. 1992; Orf et al. 1996,1999); and full cloud models, in which the life cycle of a microburst-producing storm is modeled (e.g.,Tuttle et al. 1989; Knupp 1989; Hjelmfelt et al. 1989; Straka and Anderson 1993; Parsons and Weisman 1993; Proctor and Bowles 1992; Guo et al. 1999).

Alahyari and Longmire (1995) simulated microbursts in a laboratory tank by releasing a dense volume of fluid into a less dense ambient fluid.

Full cloud models and subcloud models have been used successfully to help one to understand the microburst phenomena. Because cloud models with detailed cloud microphysics are useful to reproduce the full life cycle of a microburst-producing storm and to illustrate the mechanisms of initiation of downburst from dynamical and microphysical processes and their interactions, as well as the effect of environment on formation of microburst, and while subcloud models are used to study the detail structure of microburst itself with higher resolution by relying on some sort of a priori forcing to initialize the microburst rather than the whole storm. Generally, not any environmental shears are included in these models.

Microburst phenomena have been often found in Japan Island due to developing of radar observational system and it aroused more and more researcher's interests (Kobayashi and Kikuchi,1989; Shirooka and Uyeda.,1991; Tabata and Akaeda et al.,1991; Ohno and Suzuki et al.,1993,1994; Takayama and Niino et al.,1997).

In this study, a three-dimensional cloud model was used to reproduce a strong downburst-producing hailstorm and to investigate the possible mechanism which leaded to the down-

burst.

On September 8 1994, a severe long-lasting thunderstorm associated with hail and a strong gusty wind passed over the Gunma and Saitama prefecture and produced serious damage to window glass in a high school and injured 2 teachers and 71 students. Analysis of available data observed during that time show that downbursts should be responsible for the accident (Takayama and Niino et al.,1997, hereafter referred to as TN97).

2. The Model

The model used in this study is same as that used by Guo (1997), and Guo and Niino et al.(1999). The coordinates of the model are the standard Cartesian coordinates (x,y,z). The independent variables of the model are the velocity components u,v and w in the x, y and z directions, respectively, pressure p, potential temperature θ, mixing ratio of water vapor q_v, bulk cloud water q_c, bulk cloud ice q_i, bulk rain water q_r, bulk snow aggregates q_s and ice concentration N_i, mixing ratio of discrete mass categories of graupel/hail $q_h(I)$ for I=1, L_h, where L_h is the number of graupel/hail categories.

The model equation system is as follows:

$$\frac{du}{dt} + c_p\bar{\theta}_v\frac{\partial\pi'}{\partial x} = D_u, \tag{1}$$

$$\frac{dv}{dt} + c_p\bar{\theta}_v\frac{\partial\pi'}{\partial x} = D_v, \tag{2}$$

$$\frac{dw}{dt} + c_p\bar{\theta}_v\frac{\partial\pi'}{\partial z} = f_w + D_w, \tag{3}$$

$$\frac{d\pi'}{dt} + \frac{\bar{C}^2}{c_p\bar{\rho}\bar{\theta}_v^2}(\frac{\partial\bar{\rho}\bar{\theta}_v u_j}{\partial x_j} = f_\pi + D_{\pi'}, \tag{4}$$

$$\frac{d\theta}{dt} = Q_{mf} + Q_{ce} + Q_{ds} + D_\theta, \tag{5}$$

$$\frac{\partial q_x}{\partial t} = -D_{q_x} + W_{q_x} + I_{q_x} + \frac{\partial}{\partial x_3}(\rho_0 V_{tx} q_x), \tag{6}$$

where

$$f_w = g(\frac{\theta'}{\bar{\theta}} + 0.608q_v' - q_c - q_r - q_i - q_s - \sum_{I=1}^{L_h} q_g(I)), \tag{7}$$

$$f_\pi = -\frac{R_d}{c_v}\pi\frac{\partial u_j}{\partial x_j} + \frac{C^2}{c_p\theta_v^2}\frac{d\theta_v}{dt}. \tag{8}$$

D_u, D_v, D_w, D_θ and D_π are the turbulent fluxes of u, v, w, θ and π, respectively. Q_{fm}, Q_{ce} and Q_{ds} are the latent heating/cooling terms in association with melting/freezing, condensation/evaporation, and deposition/sublimation produced by microphysical processes, respectively. W_{q_x} and I_{q_x} are cloud microphysical sink and source terms which are related to warm and cold rain processes. V_{tx} is the terminal velocity of a hydrometeor q_x, where q_x is one of the mixing ratios of water vapor q_v, cloud water q_c, rain water q_r, cloud ice q_i, snow q_s, and hail/graupel category water content $q_g(I)$. In this paper, L_h was assumed to be 21. V_{tx} for cloud water was assumed to be zero and for cloud ice was considered to be the function of its mean diameter(Locatelli and Hobbs,1974).

To overcome the shortcomings in calculation of cloud ice number concentration using relationship with temperature, Cloud ice number concentration N_i was also predicted based on a concentration equation in this study (Guo et al. 1998).

The model includes a conventional first-order closure for subgrid turbulence and a diagnostic surface boundary layer based on Monin-Obukhov similarity theory. The equations are solved numerically using finite-difference methods on a rectangular grid. The model variables are staggered using Arakawa C-grid system with scalars defined at the center of the grid boxes and the normal velocity components defined on the corresponding box faces.

Time integration of governing equations of the compressible atmosphere uses a conventional time-splitting technique (Klemp and Wilhelmson, 1978): a short time step 0.0625 seconds is used for acoustically active terms, while a large time step of 5 seconds is used for the remaining terms. The large time-step integration uses a standard second-order leap-frog scheme. To prevent separation of numerical solutions deduced by second-order frog-leap scheme, an Asselin (1972) time filter is used in the model.

With the exception of the advections terms which are fourth-order accurate, the spatial difference terms are second-order accurate. In addition, fourth-order and vertical second-order spatial filters in the horizontal and vertical directions are used for all variables except for pressure to damp grid scale noise due to nonlinear instability.

The lateral boundaries use a radiation boundary scheme suggested by Klemp and Wilhemson (1978). The rigid top and bottom boundary conditions with an upper boundary Rayleigh damping layer which absorb upward propagating wave disturbances and eliminate wave reflection at the top boundary are used in the model.

3. Microphysical processes

There are two important improvements included in the present model: one is that the size distribution of hail/graupel is not prescribed, but is allowed to evolve naturally through mass category technique proposed by Berry (1967). Second, an equation for number concentration of ice crystal is included besides the one for its mixing ratio considering the important role of ice crystal particles playing in cold cloud (Hobbs,1974; Guo et al. 1998).

Important microphysical processes included in this model are: the melting of snow and hail/graupel; evaporation of rain; the accretion of rain by snow and hail; the shedding of water from melting of snow and hail; the sublimation of water vapor from snow and hail/graupel and the evaporation of liquid water from melting of snow and hail/graupel and the evaporation of liquid water from melting of snow and hail/graupel. The terminal velocities for rain and snow are computed as mass mean-weighted values while hail/graupel with a certain diameter (or category) falls at a terminal velocity given by Wisner et al. (1972).

3.1 Model initialization

The model atmosphere has an initial profiles which was synthesized from the upper air soundings at Maebashi and Tateno stations. Maebashi station is nearer to the area of occurrence of downburst and is to be considered as the most representive environment for bearing this downburst-producing storm. Due to lacking of soundings of wind data in Maebashi, the wind data of Tateno at the same peorid was used in the simulation. The storm passed over the area between Gumma and Saitama prefectures at 0500JST 8 September 1994.

The domain size for the simulation was 36 km ×36 km in the horizontal and 19 km in the vertical. The grid interval was 500m in both horizontal and vertical directions. The simulation was initialized by a thermal bubble with size 8 km × 8 km in the horizontal and 2 km placed at the center of the model domain (Klemp and Wilhelmson,1978). The peak temperature perturbation at the center of the thermal bubble was 4 K.

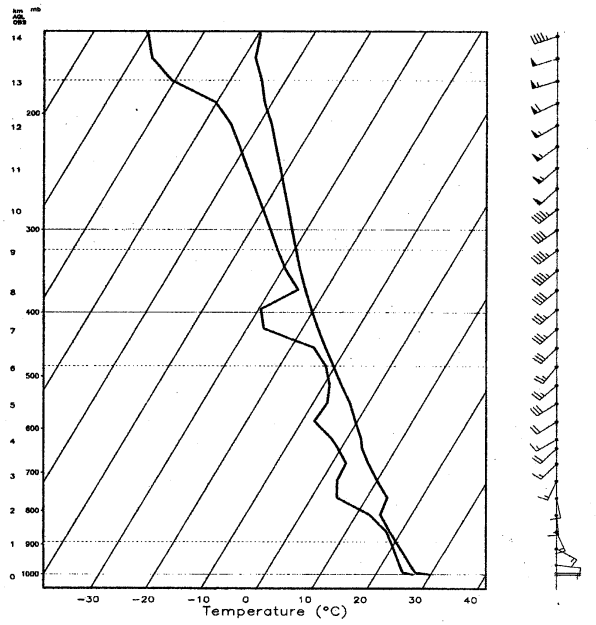

Fig.1 Skew T-logp diagram for temperature and dewpoint temperature observed 0500JST 8 September 1994 Japan.

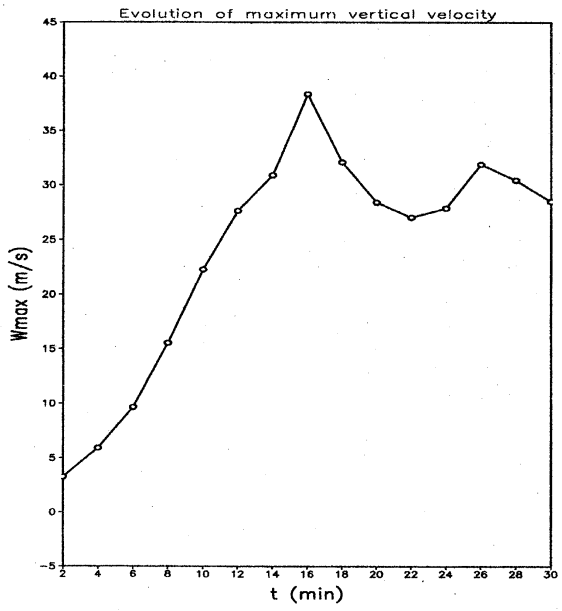

Fig.2 Peak simulated updraft velocity (m/s) vs time (min).

4. Results

4.1 Storm environment

This microburst-producing storm occurred while a cold front originally extending from a low over the Sea of Okhotsk passed over the Japan Islands and moved toward the Pacific Ocean. During the moving of the cold front over the northern part of the Japan Sea , a line-shaped cloud area was detected by both an infrared image of GMS-4 and a Mt. Fuji radar after 1200JST on 8 September 1994. At 500 hPa level, a trough moved over the Japan Sea and accompanying cold-air intruded into the north and east parts of Japan in the afternoon of that day.

The storm which produced hail and microbursts started to develop along the line-shaped cloud area. When the storm moved to the border of Gunma and Saitama prefectures, the lowest temperature at cloud-top reached about −65.0°C which corresponded to about 15 km AGL according to the sounding data at Maebashi. The damaging wind near the surface estimated from the general damage characteristics in that area reached more than 50 ms^{-1}. The storm was produced in the environment with the surface temperature of about 30°C and surface dewpoints of about 26.8°C.

The temperature sounding at 0500JST was characterized by an extremely deep moist-adiabatic layer from the top of boundary to near the tropopause. In the boundary layer, it showed a stable layer with temperature lapse rate being about 6°Ckm^{-1} and lapse

rates of water vapor mixing ratio being $4gkg^{-1}km^{-1}$. The vertical profile of moisture exhibited a relatively wet atmospheric boundary layer and relatively dry middle layers. So the moist condition would be more conducive to wet-microburst generation. The mountain orography along Saitama area might help generate convective thunderstorm in moist sounding condition. The lifted condensation level(LCL) was near 950 hPa and the lifted indices (LI) was $-7°C$. But the atmosphere was in the most unstable condition with CAPE about 3243 $m^{-2}s^{-2}$ and with a relatively strong vertical wind shear just before the occurrence of storm due to strong surface heating.

The present temperature sounding also included a very typical upper-air inversion layer. It was found that the temperature profile prior to severe weather formation typically shows a temperature decrease with height from the surface to about 800 hPa followed by a temperature increase with height for a short distance and then a temperature decrease again. The presence of an upper air inversion generally suppresses the development of cloud until a thermal, or small cloud is able to break through the inversion layer. This delay frequently allows the resulting thunderstorm to grow much larger than ordinary because the stable inversion layer prevents initial thunderstorm development. The delayed cloud development lets the sunlight continue to warm the ground and lower atmosphere until a bubble of air is so much warmer than the air above the inversion layer that much more violent thunderstorm form.

4.2 Evolution and storm structure

Time evolutions of maximum updraft of simulated storm is shown in Fig.2. The evolution and intensity of the simulated storm was almost consistent with the observed one. The simulated storm developed rapidly, with peak updraft as large as $40ms^{-1}$. Maximum updraft strength occurred 16 min after initialization as shown in figure 2 , which was consistent with the simulations of COHMEX (Straka and Anderson,1993) and at an altitude of 7 km above the ground. After reaching peak updraft strength, the simulated storm did not collapse immediately instead exhibited some degree of weak updraft redevelopment. This corresponded to the long-lived feature of observed storm. A time sequence of hail specific water content (larger than 5g/kg) and vertical velocities is depicted in west-east vertical cross sections taken near the center of the modeled storm is shown in Fig.3. The first downburst with a peak divergent wind speed of over 50 m/s at surface occurs in association with strong descending motion of precipitation core. Because the weakening updraft and strong vertical shear, a very obvious overhang, located between 2-9 km AGL, extends eastward from the main precipitation shaft. Following 26 min, precipitation begins to fall from the overhang, reaching the ground after 28 min and producing a second downburst.

The simulated obvious precipitation core descending process and overhang structure are well consistent with observations by the Mt. Fuji radar. Observations shows that the storm had a marked overhang in the direction of its movement and an obvious descent of reflecting core which was speculated to be caused by falling hail(TN97). Hail and graupel are first formed in upper part of storm at 14 min and then it enteres a very quick developing stage (16 min in Fig3). At about 17-18 min , the hail core reaches the ground after 4 min from its formation stage. The speed of descent of hail core between 16 min-18 min is roughly estimated to be about 2000 m / 120 s = 16.7 m/s which equals to the estimated speed of the descent of the reflecting core observed by radar. The storm starts to tilt due to strong vertical shear and weakening updraft after reaching the maximum

stage of updraft (20 min in Fig.3). So the radar could detect a strong overhang in its moving direction. With the development of overhang, the precipitation starts to fall from the overhang (26 min Fig.3) and finely reaches the ground (30 min in Fig.3).

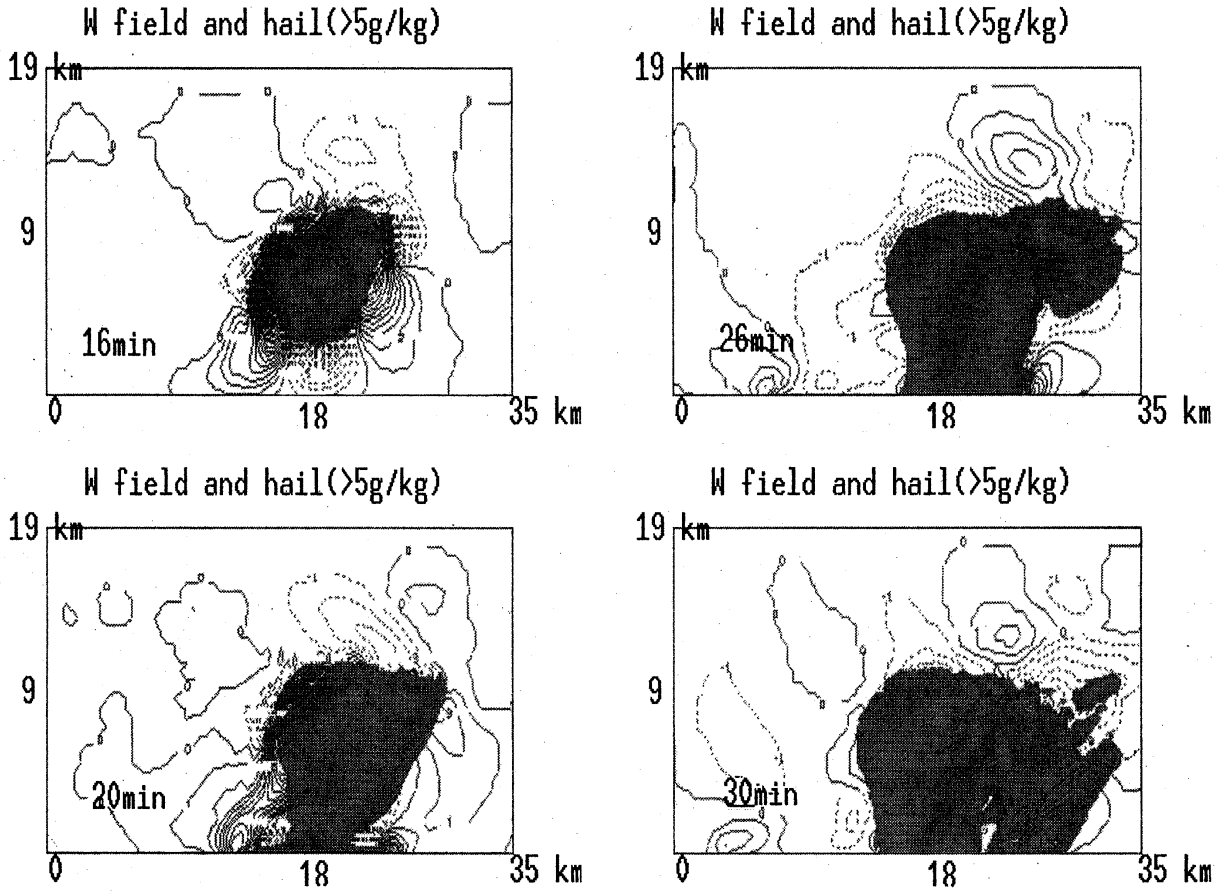

Fig.3 The evolution of specific water content of hail and vertical velocities in vertical cross-section for the simulated microburst-producing storm (shaded area indicates the hail specific water content larger than 5.0 g/kg.

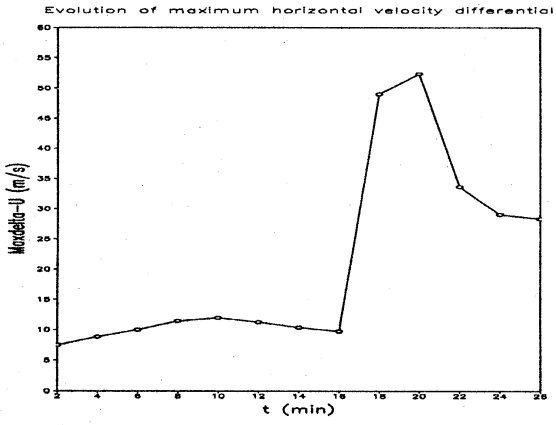

Fig.4 Peak simulated divergent velocity (m/s) vs time (min) at the surface.

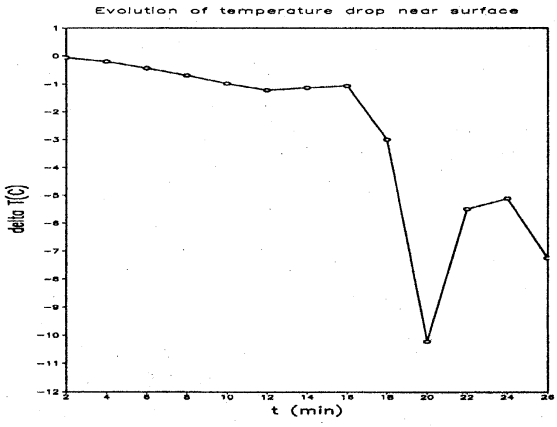

Fig.5 Peak simulated temperature drop vs time (min) at the surface.

The divergent wind speed and temperature at the surface express abrupt change accompanied with hail descending process. Figure 4 and 5 show time series (min) of peak divergent wind speed and temperature deviation at surface,respectively.

4.3 Downdraft development

A time series of downdraft velocities (less than -10 m/s)(Fig.6) shows that a weak downdraft first forms at the upper part of storm in association with hail formation (16 min in Fig.6, see also Fig.3) at the height of 8 km AGL. It takes about 4 minutes for the downdraft to reach the ground and produces the strongest surface microburst. At 20 min it entered mature stage with a obvious tilting structure for both updraft and downdraft. The downdraft had a diameter of about 3-4 km, which corresponding to precipitation shaft. The downdraft became weak after 22 min and entered a dissipating stage. At 24 min, the second downburst started to develop, and after 6 min, it reached the surface (30 min).

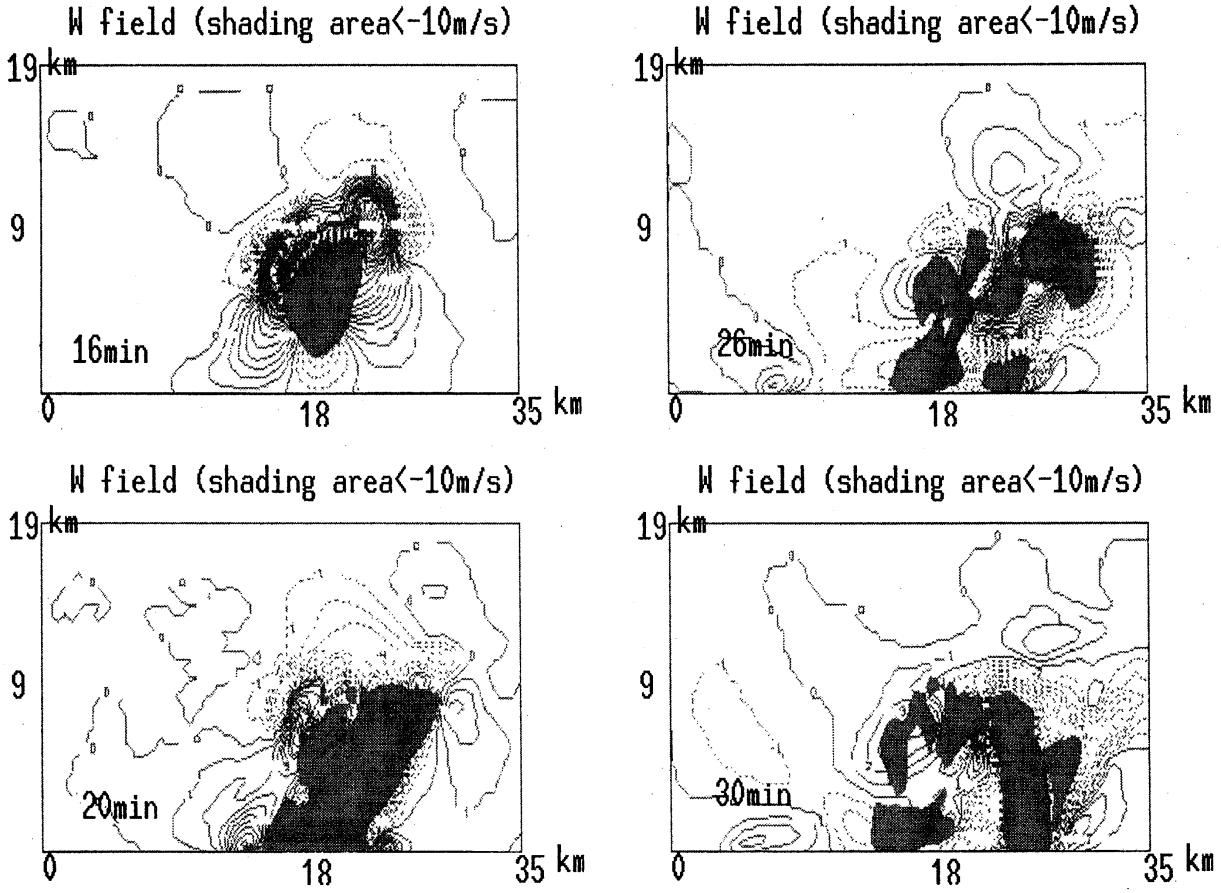

Fig.6 The evolution of downdraft and vertical velocities in vertical cross-section for the simulated microburst-producing storm (shaded area indicates the downdraft less than -10m/s)

The size of low-level downdraft in the simulated storm was about 4 km in diameter. The downdraft originated below the melting level(4.7 km AGL). The simulated peak downdraft velocity of -90 m/s occurred in the layer between 1.5-2.0 km AGL at 18 min 2 min after the storm attained maximum updraft (Fig.7 and Fig.8).

The formation of the simulated downdraft well coincided with the descending hail core (Fig.7), hail accompanied the arrival of the downdrafts at the surface. After passing

through the 0^0C level, the downdraft producing from loading of hail decreases because of decreasing of hail content due to melting process while the downdraft producing from melting of hail and evaporation of rain increases . So there is an obvious time lag for maximum downdraft near 0^0C layer. With increasing of temperature, the downdraft increases due to increasing of melting and evaporation above 2.0 km AGL. There is a maximum core of downdraft near 2.0-2.5 km AGL. But the maximum downdraft decreases with increasing of temperature below 2.0 km AGL.

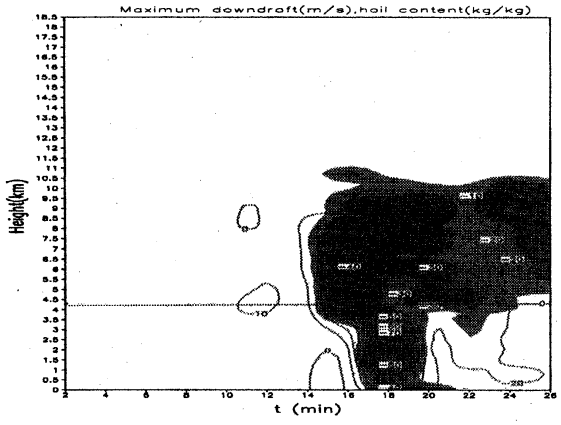

Fig.7 The hight-time distribution of maximum downdraft (m/s) (dotted line) and hail specific water content (kg/kg) (shaded area larger than 0.02 kg/kg).

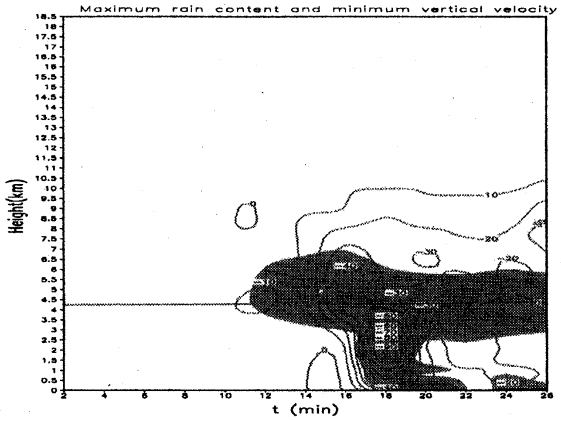

Fig.8 The hight-time distribution of maximum downdraft (m/s) (dotted line) and hail specific water content (kg/kg) (shaded area larger than 0.02 kg/kg).

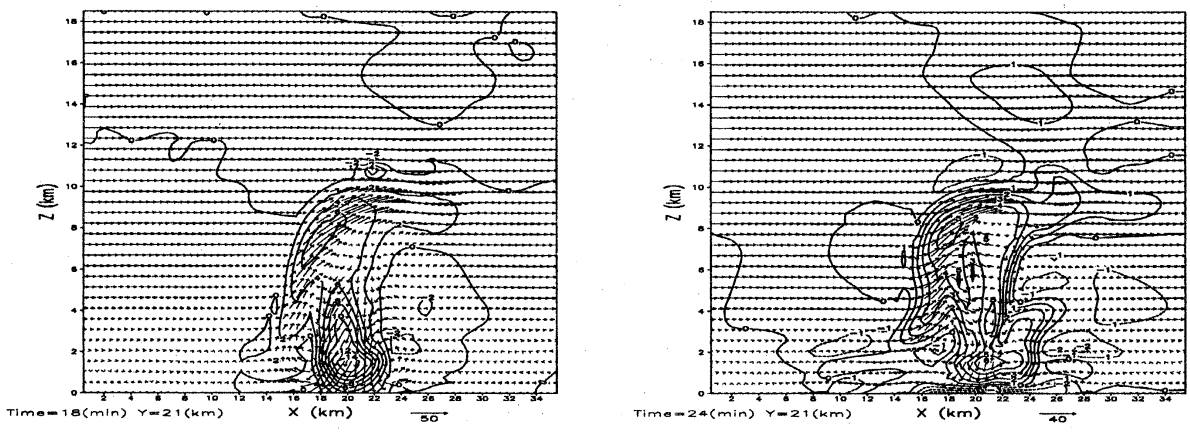

Fig.9 The vertical cross-section of distribution of temperature deviation.

As we know, the evaporation of rain and melting of ice tend to cool the air, while the descending motion tends to warm it. From the distribution of temperature difference between downdraft and environment (Fig.9), it shows the entire region of the downdraft is warmer than its environment, especially in the region below 0^0C layer during the mature stage of first downburst (18 and 20 min). This because the descending compressional warming dominates in contrast with the effect of evaporative and melting cooling. The cooling process due to strong melting and evaporation accelerates the descending motion of downdraft. But at same time, the stronger downdraft has stronger warming effect

which produces the positive thermal buoyancy to decelerate the descending motion of downdraft. So the maximum core of downdraft locates at the 2.0 km AGL in Fig.7 other than at the surface. From 24 min, a region of deficit temperature start to present near the surface due to the domination of the effect of cooling of evaporation and melting in the region.

The distribution of rain content was mainly due to the melting of hail and the maximum rain content located near surface will be very important to enhance the intensity of divergent wind speed through strong evaporative cooling process (Fig.8).

4.4 Development of surface outflow

In the simulation, a dome of high pressure began to develop at 16 min at the surface 2 min prior to the development of divergent surface outflows (18 min). Maximum high pressure at the surface occurred at 18 min corresponding to the time of the strongest downdraft. The maximum amplitude of the surface high pressure was about 20 mb (Fig.10) and it is much larger than that previous cases of microbursts (Straka and Anderson,1993).

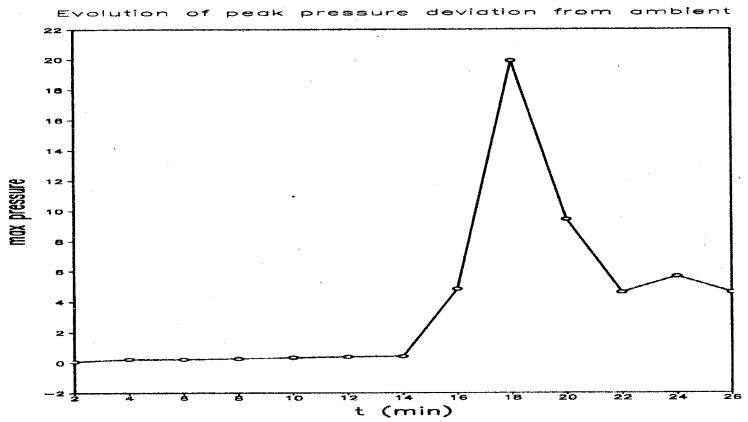

Fig.10 Peak pressure deviation near the surface.

Knupp (1989) and others have shown that microbursts are forced by strong horizontal pressure gradients near surface. Based on damage characteristics, the maximum wind speed was estimated to be about 50 m/s (F1) in present case (TN97). So the maximum amplitude of surface pressure should be much larger than that of ordinary cases. The simulated surface outflow was confined to the lowest one layer in the model (500m), and peak differential velocity occurred in the first model layer.

The structure and degree of symmetry in the simulated surface outflows can be seen in the surface wind vector fields in Fig.11. It shows that the simulated surface outflows are almost symmetric at initial stage (20 min) and become asymmetric during its development (30 min). Hjelmfelt (1988) found that some microbursts asymmetries might be apparent in nature and result from the superposition of a subcloud mean flow on a symmetric outflow. Straka and Anderson (1993) studied the correlation between the aspect ratio of surface outflows and vertical shear of low levels of the environmental winds and suggested that a vertical shear of the environmental winds, through the layers where hydrometeors form, might produce an asymmetry in a storm's low-level outflow.

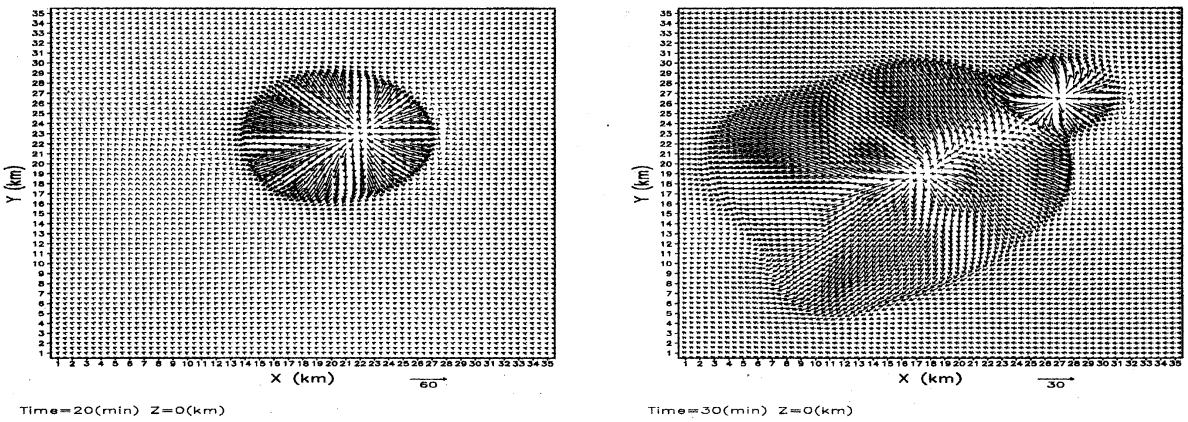

Fig.11 The wind vector distribution in association with downburst near surface.

For the current simulation, a downshear tilting of downdraft due to vertical shear in the environmental wind can be seen clearly. A more detailed analysis of the asymmetrical surface outflows is outside the scope of this study.

4.5 Microphysical forcing of downdrafts

As mensioned above, many researchers such as Srivastava (1985,1987), Krueger et al (1986), Proctor (1988,1989), Knupp (1989), Tuttle et al(1989), Orville et al. (1989), Hjelmfelt et al. (1989), and Straka et al. (1993) have demonstrated that the importance of hydrometeors in the development of downdrafts through changes in buoyancy due to loading and heat loss associated with water phase changes.

Srivastava (1987) suggested that the rapid cooling associated with the melting of small ice particles could be important in the production of intense downdrafts, especially when the atmosphere is stably stratified.

It was shown from the studies by Orville et al. (1989) and Knupp (1989) that loading effects of hail were largest above the melting level, cooling by melting of hail was greatest at a height midway between the ground and the melting level, and cooling by evaporation of rain was greatest at 1 km of the ground. The numerical simulation described by Krueger et al. (1986) and Proctor (1989) indicated that the cooling associated with phase changes of various hydrometeor types can influence surface outflow strength and low-level downdraft strength. However it should be noted here that the sensitivity tests done by Krueger et al. (1986) and Proctor (1989) were concerned with downdraft production below cloud base and that the influence of ice physics on the evolution of the parent storm was not considered.

In a numerical simulation of a microburst-producing storm, Hjelmfelt et al.(1989) showed that switching off the cooling associated with evaporation of rain and melting of hail in regions of low-level downdrafts substantially reduced surface outflow strength. He also showed that switching off the formation of graupel/hail significantly influenced the evolution of the storm, the formation of rain, the intensity of low-level downdrafts, and the strength of the surface outflow. The simulations of microburst-producing storms by Straka et al. (1993) showed that low-level downdrafts are in some cases stronger and deeper in simulations with the ice phase than in those without the ice phase.

To examine the influence of microphysics in the production of downdrafts in the simulations of thunderstorm occured on September 8 1994 in Japan, downward acceleration rates

due to hydrometeor loading and cooling associated with phase changes were calculated following the formulation by Hjelmfelt (1989) and Orville et al. (1989).

A simplified form of vertical equation of motion is differentiated with respect to time, and is written as

$$\frac{\partial}{\partial t}(\frac{dw}{dt}) = \frac{g}{\Theta}(\frac{\partial \theta'}{\partial t} - \Theta\frac{\partial q}{\partial t}) + ... \tag{9}$$

where w is the vertical motion, g gravity, t time, q the total condensate mixing ratio, θ' temperature or potential temperature deviation from a base state Θ, respectively. The temperature changes due to melting and evaporation are given by

$$(\frac{\partial \theta'}{\partial t})_{melting} = \frac{L_f}{c_p}(\frac{\partial q_h}{\partial t})_{melting} \tag{10}$$

and

$$(\frac{\partial \theta'}{\partial t})_{evaporation} = \frac{L_v}{c_p}(\frac{\partial q_r}{\partial t})_{evaporation}, \tag{11}$$

respectively, where L_v and L_f are the latent heats of fusion and evaporation, respectively; q_h is the mixing ratio of graupel/hail and snow; q_r is the mixing ratio of rain; and c_p is the specific heat at constant pressure.

To analyze the temperature change term in (10) and (11), it is necessary to know the rates of changes in hail/graupel, snow and rain due to melting (or freezing) and evaporation. Similarly, it is also necessary to know the time rate of change in the loading of hail/graupel, snow and rain and multiply by Θ to evaluate the effect of that term in (11). As an example, a constant cooling rate of $1°C min^{-1}$ causes an acceleration of -0.096 ms^{-2} in 3 min and a vertical velocity of -8.64 ms^{-1}, assuming zero initial acceleration and vertical velocity. Temperature deficites of $1°C$ and precipitation loads of 1 gkg^{-1} produce accelerations of -0.033 and -0.01 ms^{-2}. If constant, and with the same assumptions as above, these values produce vertical velocities of -6.0 and -1.8 ms^{-1} respectively, in 3 min. When the downdraft hits the ground, the horizontal pressure gradient term becomes the most important as shown above. Numerical simulation show extreme values of 1 mb excess over 200 m in a very strong microburst case, giving an acceleration of $0.4ms^{-2}$ for a short while and yielding large changes in the horizontal motion. Based on the result, peak pressure deviation of more than 20 mb near the surface would produce a very strong horizontal motion.

The time-height distribution of maximum cooling rates is given in Fig.12. All variables shown on figures are the maximum values in the downdraft region. At the time of downdraft initiation (16-18 min),the largest acceleration rate which is equivalent to about $14.0°C/min$ is due to graupel/hail loading near the height of 6.5 km AGL (Fig.12a). This illustrates the role of loading by the graupel/hail field in initiating the downdraft above the melting level. Below the melting level, graupel/hail melting acceleration rates become the most important term to the producing of strong downdraft.

The maximum acceleration rates due to hail/graupel melting is located near 2-2.5 km AGL near the time of the maximum downdraft occurrence. So the primary mechanism for the downdraft acceleration in the layer between 2 and 3 km AGL immediately beneath the 0°C level is the cooling produced by melting of graupel/hail. There are two maximum centers for hail/graupel melting acceleration rates: the first one of about $16.0°C/min$ is

located near 2-2.5 km AGL and occurred at 18 min, about the time of the maximum downdraft (Fig.12b). The second one is located near the surface at 20 min, the time of maximum outflow velocity at the surface.

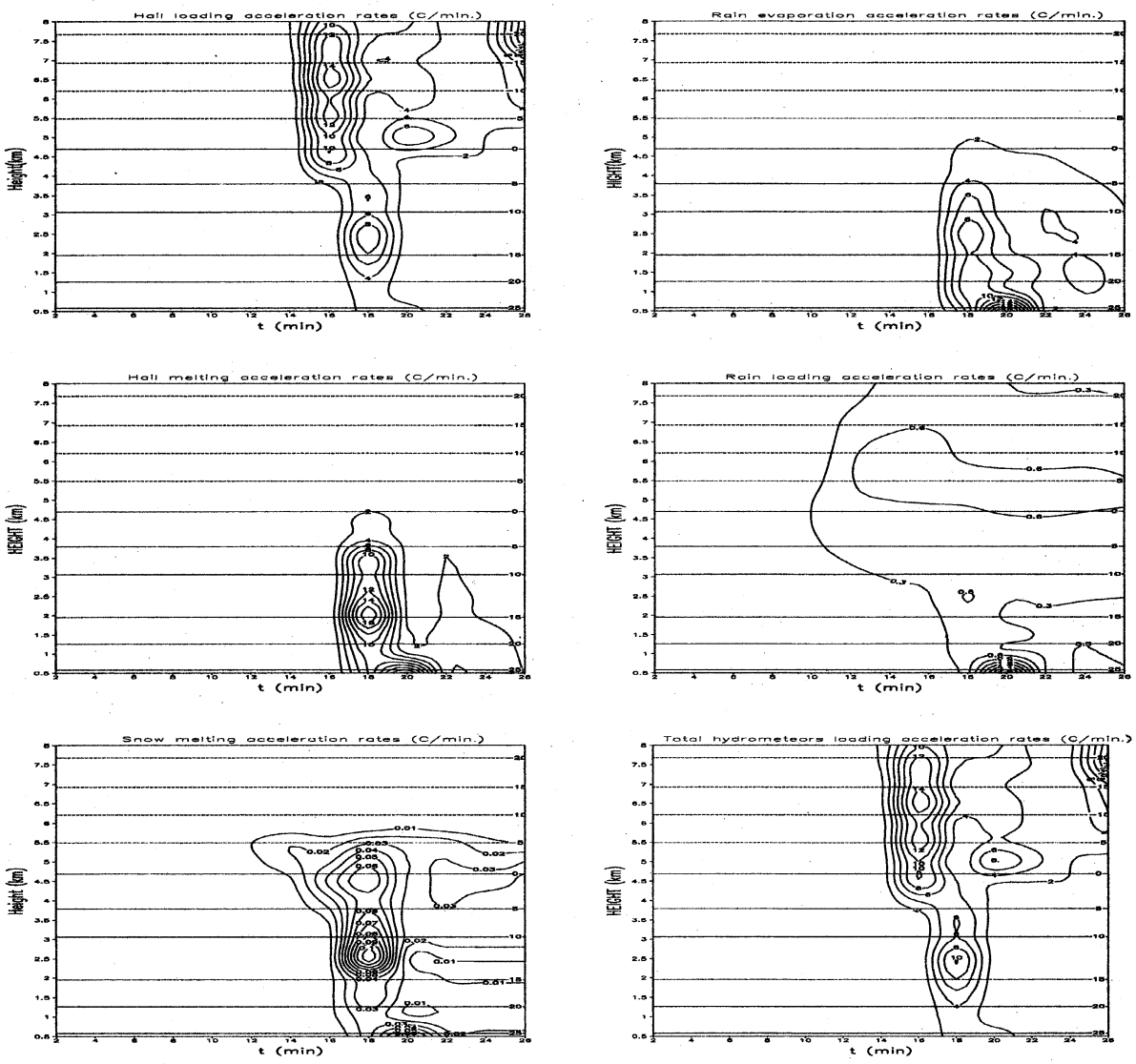

Fig.12 The time-height distribution of maximum magnitude of effective cooling rates for forcing mechanisms due to a) hail loading, b)hail melting, c)snow melting, d) rain evaporation, f) rain loading, e) the sum hydrometeor loading.

The snow melting acceleration rates is very small compared with hail/graupel (Fig.12c). The second largest acceleration mechanism between 1 and 3 km AGL is the evaporative cooling (Fig.12d). Evaporation increases as rain reaches the ground. At 20 minutes, evaporation near surface attains the maximum as the rain falls out. Although the cooling due to evaporation at low levels is not able to produce a strong downdraft, it may contribute to strength of the outflow through enhaced horizontal pressure gradient force (Krueger et al. 1986).

The rain loading acceleration rates was only important near the surface (Fig.12 e). This is because the most rain is produced from hail melting. Comparing hail loading acceleration rates (Fig.12a) with total hydrometeors loading rates (Fig.12f), one can find

that a majority of loading is due to hail.

In summary, the downdraft in the storm is initiated primarily as a result of graupel/hail loading. Melting of graupel/hail into rain below 0° level then importantly contribute to the development and acceleration of the downdraft. A relatively large cooling rates due to evaporation occurrs at low altitudes and enhances the microburst outflow intensity. The maximum cooling rates due to evaporation just occurs at the time of microburst. So graupel/hail is of vital importance in microburst producing storm.

5. Summary and discussion

This paper first used a three-dimensional hail category, nonhydrostatic cloud model to make simulation of a strong microburst-producing storm on 8 September 1994 based on rawinsonde sounding from Maebash and Tateno of Japan. Using a grid resolution of 500 m, there was fair agreement in the characteristics of observed and simulated microburst strength, lifetime, surface precipitation and hailfall size. Furthermore, strong low-level downdrafts and outflows in the simulation were preceded by a peak in hail concentration, a descending precipitation core, and convergence beneath the melting level (figure is not shown). In addition, multiple microburst production was also captured in the simulation. The formation of graupel/hail was important to the precipitation process and to the formation of rain and downburst in the model.

Simulation results suggested that the production of downburst of the storm on 8 September 1994 in Japan can be explained by the effects of negative buoyancy initiated by graupel/hail loading and enhanced by the cooling due primarily to the melting of graupel/hail and evaporation of rain, which is similar to the results of Srivastava (1985,1987), Proctor (1988), Hjelmfelt (1987), Hjelmfelt et al. (1989), Krueger et al. (1986) and Straka et al. (1993). This simulation also illustrate that hail category numerical model can provide realistic simulations of very strong microburst production from simulated storm based on the observed enviromental conditions using a relatively larger grid size resolution. But this does not mean that any grid resolutions are feasible. Adequate grid resolution is still needed. In fact, the same calculation with 1 km grid interval did not produce microbursts of observed strength.

References

Asselin, R., 1972: Frequency filter for time integrations. *Mon. Wea. Rev.*,**100**, 487-490.

Alahyari, A., and E. K. Longmire,1995: Dynamics of experimentally simulated microbursts. *AIAA J.*, **33**,2128-2136.

Anderson, J. R., L. G. Orf, and J. M. Straka,1992: A 3-D model system for simulating thunderstorm microburst outflows.*Meteor. Atmos. Phys.*,**49**, 125-131.

Berry, E. X.,1967: Cloud droplet growth by collection. *J. Atmos. Sci.*,**24**, 688-701.

Fujita, T.T.,and F.Caracena, 1977: An analysis of three weather-related aircraft accidents. *Bull. Amer. Meteor. Sco.*,**58**, 1164-1181.

Fujita,T.T., 1981: Tornadoes and downbursts in the context of generalized planetary scales. *J. Atmos. Sci.*,**38**, 1511-1534.

Fujita, T. T., 1983: Andrews AFB microburst. SMRP Res. Pap. 156, University of Chicago, Dept. of Geophysical Sciences, Satellite and Mesometeorology Research Project, 104 pp.

Fujita,T. T., 1985: The downburst: Microburst and macriburst. Satellite and Mesometeorology Research Project, Research Pap. No. 210, University of Chicago, 122pp.

Guo X. L., 1997: The studies on three-dimensional hail category numerical simulations of hail formation and hailfall processes, Ph.D Thesis,*Institute of Atmospheric Physics,Chinese Academy of Sciences.*

Guo X. L., Y. S. Chung, M. Y. Huang and L. Zhou, 1998: Raindrop category numerical modeling on microphysical process of precipitation formation of stratiform cloud in northern China. *J. of Korea Meteor. Soc.*,**34**,613-623.

Guo X. L., H. Niino and R. Kimura, 1999: Numerical simulation of a microburst- and hail-producing storm on 8 September 1994 in Saitama Prefecture. Preprints. 4rd Symposium on Environmental Fluid Mechanics ,*Japan Soc. Fluid Mech.*, 501-502.

Hobbs, P. V., 1974: High concentrations of ice particles in a layer cloud, *Nature*,**251**,694-696.

Hjelmfelt, M. R., H. D. Orville, R. D. Roberts, J. P. Chen, and F. J. Kopp, 1989: Obervational and numerical study of a microburst line producing storm. *J. Atmos. Sci.*,**46**, 2731-2743.

Krueger, S. K., R. M. Wakimoto, and S. J. Lord, 1986: Role of ice phase microphysics in dry microburst simulations. Preprings, 23rd Radar Meteorology Conf., Snowmass, *Amer. Meteor. Soc.*, R73-R76.

Klemp, J. B., and R. B. Wilhelmson, 1978: The simulation of three-dimensional convective storm dynamics. *J. Atmos. Sci.*,**35**, 1070-1096.

Knupp, K. R., 1989: Numerical simulation of low-level downburst initiation within precipitating cumulonimbi: Some preliminary results. *Mon. Wea. Rev.*,**117**, 1517-1529.

Kobayashi,F. and K. Kikuchi, 1989: A microburst phenomena in kita Village, Hokkaido on September 23, 1986. *J. Meteor. Soc. Japan*,**67**, 925-936.

Orville, H. D., R. D. Farley, Y-C. Chi, and F. J. Kopp, 1989: The primary cloud physics mechanism of microburst formation. *Atmos. Res.*,**24**, 343-357.

Ohno, H.,O. Suzuki, K. Kisunoki, H. Nirasawa and K. Nakai, 1993: A severe downburst in Mito city on 4 September 1992. Preprints, 26th Conf. on Radar Meteorology, Norman, Oklahoma, *Amer. Meteor. Soc.*, 221-222.

Ohno, H.,H. Nirasawa, M. Yoshizaki, N. Hasegawa ,Y. Tanaka, Y. Muramatsu and Y. Ogura, 1994: Okayama downbursts on 27 June 1991: Downburst identifications and enviromental conditions. *J. Meteor. Soc. Japan*,**72**, 197-222.

Orf, L. G., J. R. Anderson, and J. M. Straka,1996: A three-dimensional numerical analysis of colliding microburst outflow dynamics. *J. Atmos. Sci.*,**53**,2490-2511.

Proctor, F. H., 1988: Numerical simulation of an isolated microburst. Part I: Dynamics and structure. *J. Atmos. Sci.*, **45**, 3137-3160.

Proctor, F. H., 1989: Numerical simulation of an isolated microburst. Part II: Sensitivity experiment. *J. Atmos. Sci.*, **46**, 2143-2165.

Proctor, F. H., and R. L. Bowles,1992: Three-dimensional simulation of the Denver 11 July 1988 microburst-producing storm. *Meteor. Atmos. Phys.*,,**49**,107-124.

Parsons, D. B., and M. L. Weisman,1993: A numerical study of a rotating downburst. *J. Atmos. Sci.*, **50**,2369-2385.

Srivastawa, R. C., 1985: A simple model of evaporatively driven downdraft: Application to microburst downdraft. *J. Atmos. Sci.*,**42**, 1004-1023.

Srivastawa, R. C., 1987: A model of intense downdrafts driven by the melting and evaporation of precipitation. *J. Atmos. Sci.*,**44**, 1752-1773.

Straka, J. M. and J. R. Anderson, 1993: Numerical simulation of microburst-producing storms: Some results from storms observed during COHMEX. *J. Atmos. Sci.*,**50**, 1329-1348.

Shirooka, R. and H. Uyeda, 1991: Doppler radar observation of tornado and microburst around Chitose airport. Preprints, 25th Conf. on Radar Meteorology, Paris, *Amer. Meteor. Soc.*,J73-J76.

Takayama H., H. Niino, S. Watanabe, J. Sugaya et al., 1997: Downbursts in the northwestern part of Saitama prefecture on 8 September 1994. *J. Meteor. Soc. Japan*,**4**, 885-905.

Teske, M. E., and W. S. Lewellen, 1977: Turbulent transport model of a thunderstorm gust front. Preprints, 10th Conf. on Severe Local Storms, Omaha, *Amer. Meteor. Soc.*, 143-150.

Tuttle, J. D., V. N. Bringi, H. D. Orville, and F. J. Kopp, 1989: Multiparameter radar study of a microburst: Comparisons with model results. *J. Atmos. Sci.*,**46**, 601-620.

Tobata, A., K. Akaeda, M. Ishihara and H. Sakakibara, 1991: Structure of downbursts associated with heavy rainfall observed in Tokyo. Preprints, 25th Conf. on Radar Meteorology, Paris, *Amer. Meteor. Soc.*, J177-J80.

Wilson, J. W., J. A. Moore, G. B. Foote, B. Martner, A. R. Rodi, T. Uttal and J. M. Wilczak, 1988: Convection Initiation and Downburst Experiment (CINDE). *Bull. Amer. Meteor. Soc.*, **69**, 1328-1348.

Wisner, C. H., H. D. Orville and C. G. Myers, 1972: A numerical model of a hail-bearing cloud. *J. Atmos. Sci.*,**29**, 1160-1181.